https://doi.org/10.5194/egusphere-2026-6723
Preprint. Discussion started: 12 November 2026
© Author(s) 2026. CC BY 4.0 License.

# The Sensitivity of Contrail Radiative Forcing to the Radiative Transfer Parameterization

Paulina Czarnecki[1], Olivier Boucher[1], and Nicolas Bellouin[1,2]

[1]Institut Pierre-Simon Laplace, Sorbonne Université, Paris, France
[2]Department of Meteorology, University of Reading, Reading, UK

**Correspondence:** Paulina Czarnecki (pczarnecki@ipsl.fr)

**Abstract.** Contrail cirrus, ice clouds produced by aircraft passing through cold, supersaturated air, may account for over half of radiative forcing caused by aviation. Because shortwave and longwave radiative effects of upper-tropospheric ice clouds are opposite in sign, the net contrail radiative forcing remains poorly constrained with an uncertainty of 70%. Previously, an uncertainty of 35% was attributed to the choice of radiative transfer code based on a model intercomparison. In this work, we reassess the diversity in contrail instantaneous radiative forcing in a modern set of radiative transfer codes using both idealized calculations and a realistic contrail outbreak. We find that forcing estimates are most sensitive to the ice optical property parameterization, and homogenizing the ice optics halves disagreement. Among codes with identical ice optical properties, diversity is largest when forcing is small because codes may disagree on the sign; conversely, diversity is smallest when the magnitude of the forcing is large. When averaged over a realistic simulation of contrail properties, larger daytime diversity contrasts good nighttime (longwave-only) agreement, with space- and time-averaged contrail radiative forcing agreement within 22%, and 11% when ice optics are homogenized. These results shows that while accounting for microphysical uncertainties remains important, the identification of the most radiatively-impactful contrails as targets for mitigation strategies is robust to the choice of radiative transfer code. Finally, in a calculation analogous to a previous benchmark, the uncertainty due to radiative transfer code is assessed at 12%, leading to an overall uncertainty of 60% in global contrail radiative forcing.

## 1 Introduction

High, thin cirrus clouds cover a significant portion of Earth's area (about 30%; Gasparini et al., 2018), and because of their low opacity, they typically radiatively warm Earth's climate (Chen et al., 2000; Liou, 1986). In addition to natural cirrus, aviation induces condensation trails, or contrails: clouds that form in moist, cold regions due to the passage of an airplane. Both contrails and natural cirrus increase the absorption of thermal radiation (at long wavelengths, or longwave radiation) and the scattering of solar (shortwave) radiation, altering Earth's energy balance. The direct radiative effect of contrails can be measured through their instantaneous radiative forcing (IRF). The sign of the net forcing is set by the balance between opposite effects at different parts of the electromagnetic spectrum. Longwave IRF is typically positive, while shortwave radiative effects increase the amount of radiation escaping to space and result in a negative IRF. The magnitude of both shortwave and longwave

https://doi.org/10.5194/egusphere-2026-6723
Preprint. Discussion started: 12 November 2026
© Author(s) 2026. CC BY 4.0 License.

forcing depends on the properties of the cloud, including its temperature, its optical thickness, and how it scatters or absorbs light across the electromagnetic spectrum (its optical properties).

Like natural cirrus, though contrails may exert either a positive or negative forcing depending on their properties and the position of the sun, best estimates indicate a positive net IRF of about 111.4 mW/m$^2$ (Lee et al., 2021; Wang et al., 2023). However, the overall uncertainty surrounding contrail radiative forcing is 70% (Lee et al., 2021). This means that the yearly contrail IRF may be anywhere between half to 150% of the IRF of cumulative $CO_2$ emissions due to aviation from 1940 to 2018, which are generally well-quantified (within about 10%; Lee et al., 2021). As Earth's energy imbalance grows (Mauritsen et al., 2025) and efforts are made to decrease the environmental impacts of aviation via practices such as contrail avoidance (Teoh et al., 2020; Smith et al., 2026), it is important to not only quantify the radiative effects of contrails but to understand the sources of its large uncertainty.

Uncertainty in contrail IRF arises from many factors and can be categorized as uncertainty in the contrail radiative response as well as uncertainty in the contrail formation process (A and B uncertainties, respectively; Lee et al., 2021). Within category A, the uncertainty attributed to the choice of radiative transfer code is previously assessed at 35% (Lee et al., 2021); this estimate is based on the maximum disagreement between radiation code estimates in both longwave and shortwave IRF in an idealized single-atmosphere benchmark experiment (Myhre et al., 2009). Uncertainty is assessed in the longwave and shortwave separately because when net IRF is near zero, radiative transfer codes may disagree at which cloud properties the balance between longwave and shortwave shifts (Liou, 1986; Baran, 2012), such that small differences between codes can result in a large level of uncertainty.

Differences in IRF estimates due to the choice of radiation code can arise from approximations made for practical use in modeling contexts. These modeling choices include the spectral and geometric discretizations, or in other words, how codes sample the longwave and shortwave wavelengths and how many integration angles or streams are used. Additionally, radiation codes make assumptions about cloud optical properties, including what ice particle habit or mix of ice particle habits makes up the cloud (e.g., Baran, 2012), what particle size distribution leads to a given ice effective radius (Zhang et al., 1999), and how that effective radius is defined. However, how each of these choices contributes to the uncertainty in cirrus radiative effects in modern radiation codes remains unstudied.

The goal of this work is to consolidate contrail cirrus IRF diversity in a set of commonly-used radiation codes, described in Section 2. Here we define "diversity" as the maximum spread relative to the mean of all the calculations, because while we use different radiation codes in our analysis, they do not span the full range of possible uncertainty. We first repeat the Myhre et al. (2009) benchmark experiment (Section 3.1), showing that diversity can be minimized if identical (harmonized) ice optical properties are used by each code. Next, we characterize the sensitivity of these harmonized calculations to cloud properties and solar zenith angle (Section 3.2). Finally, we show that when IRF is averaged over realistic contrail lifetimes and associated sets of properties, a compensation of disagreements leads to a smaller overall uncertainty (Section 4). We discuss the implications of these results for the overall uncertainty in contrail IRF in Section 5.

https://doi.org/10.5194/egusphere-2026-6723
Preprint. Discussion started: 12 November 2026
© Author(s) 2026. CC BY 4.0 License.

## 2 Radiative Forcing and Code Diversity

The instantaneous radiative forcing (IRF) of a contrail or cirrus cloud is defined as the difference between net radiative flux at the top of the atmosphere (TOA) between the same atmospheric profile without (clear-sky) and with (cloudy-sky) the cloud:

$$\Delta F = [F^{\uparrow}_{cs}(TOA) - F^{\downarrow}_{cs}(TOA)] - [F^{\uparrow}_{cld}(TOA) - F^{\downarrow}_{cld}(TOA)].$$

Under this definition of net flux, the shortwave component is negative and the longwave component is positive. The net forcing is the sum of the shortwave and longwave components: $\Delta F_{net} = \Delta F_{SW} + \Delta F_{LW}$.

High-accuracy forcing calculations requires integration over many angles and wavelengths. However, this quickly becomes very computationally expensive, so most codes used for Earth systems modeling seek to reduce the dimensionality of the problem (e.g., Lacis and Oinas, 1991; Fu and Liou, 1992; Hogan and Bozzo, 2018; Pincus et al., 2019). Differences in the approach lead to different estimates of IRF (Pincus et al., 2020; Hogan and Matricardi, 2020).

We quantify this diversity as

$$D = \left| \frac{\max[\Delta F(\tau,\theta)] - \min[\Delta F(\tau,\theta)]}{\text{mean}[\Delta F(\tau,\theta)]} \right|, \quad (1)$$

where the maximum, minimum, and mean are taken over the set of radiation code estimates. The mean is additionally floored by IRF = 1 W/m$^2$, to avoid artificial amplification of the diversity via division by a small mean IRF. Because we report contrail IRF without scaling by cloud fraction, this floor is of the order of magnitude of the minimum $\Delta F$ values ($\mathcal{O}(10^{-1})$ W/m$^2$; Figs. $3-4$). An alternate approach to avoiding this artificial amplification is considering the longwave and shortwave diversity separately, as in Myhre et al. (2009); this metric is discussed in Section 5.

### 2.1 Radiation Codes

We compare four popular radiation codes: the Atmospheric Radiative Transfer Simulator ARTS (Buehler et al., 2025); libRadtran (Emde et al., 2016; Mayer and Kylling, 2005); the ECMWF Radiation Scheme ecRad (Hogan and Bozzo, 2016, 2018); and the Python interface of RRTMGP (Pincus et al., 2019). The codes serve different purposes in radiative transfer modeling. With fine spectral and angular resolution, such as those used by line-by-line codes like ARTS, calculations can be considered arbitrarily accurate (Pincus et al., 2020). Because of this, line-by-line codes are used for high-fidelity reference calculations but are impractical for large-scale modeling due to high computational expense. On the other hand, fast but less accurate parameterizations (correlated-$k$ distributions such as RRTMGP and ecRad) are intended for use in climate or weather modeling. These codes average and sort spectral information, performing radiative transfer calculations at $g$-points rather than individual frequencies. Because of this averaging, the number of $g$-points used in a correlated-$k$ distribution does not necessarily reflect the density of the spectral sampling in terms of information used for the calculation of absorption or scattering. However, the computational efficiency of the correlated-$k$ approach scales with the number of $g$-points. We briefly describe the four codes and how they differ in the solution of the radiative transfer problem in Table 1.

In all four codes, clouds are described by their ice water content (IWC) and their particle size. In the case of ARTS, the latter takes the form of a modified-gamma particle size distribution (PSD) (Petty and Huang, 2011). The shape of this distribution

https://doi.org/10.5194/egusphere-2026-6723
Preprint. Discussion started: 12 November 2026
© Author(s) 2026. CC BY 4.0 License.

is determined by three parameters: $N_0$, the intercept parameter, set by the mass of the particle; $\lambda$, the slope parameter; and $\mu$, the shape parameter. In our case, we fix $\mu = 1$ (Wolf et al., 2023) and use $\lambda$ to control the PSD to obtain the effective radius, which describes the particle size in the other three radiation codes.

The definition of effective radius we adopt is:

$$r_{\text{eff}} = \frac{3\,\text{IWC}}{4\,\rho_{ice}\,A},$$

where $\rho_{ice}$ = 917 kg/m$^3$ and the reference IWC = 1 kg/m$^3$. $A$ (in units of m$^{-1}$) is the total projected area of the particles per unit volume of air:

$$A = \frac{\pi}{4} M_2,$$

where $M_2$ is the second moment of the PSD. This definition of $r_{\text{eff}}$ matches the definition of effective radius used by other radiation codes (e.g., Hogan and Bozzo, 2016, 2018) and is chosen for more direct comparison between harmonized and unharmonized estimates.

In some cases, it is more intuitive to describe the cloud by its opacity rather than its ice water content. We adopt the cloud optical depth $\tau$ at 0.55 $\mu$m. To obtain a given optical depth ($\tau = 0.3$ in the Myhre experiment, for instance), effective radius is fixed while ice water content is varied, and the reference value is calculated by ARTS.

Finally, though it is not a radiation code by itself, we compare the Contrail Cirrus Prediction (CoCiP) Radiative Forcing Parameterization (Schumann, 2012; Schumann et al., 2012) due to its popular use in contrail modeling. Because the parameterization provides forcing estimates based on an empirical fit to libRadtran reference calculations, its ice optical properties cannot be harmonized with the other codes. The inputs of the IRF estimate are the contrail ice particle effective radius, TOA solar and thermal fluxes, the contrail temperature, the contrail optical depth, and the ice particle habit. ARTS TOA fluxes and gridbox-average optical thickness at 0.55 $\mu$m are used to define the contrail. This ensures that both the CoCiP parameterization and the offline radiation codes perform the same calculation.

### 2.1.1 Harmonization

In order to isolate diversity from the radiation code itself, we harmonize the ice optics, or prescribe identical ice optical properties in each code. Rather than prescribing spectrally-uniform properties (Myhre et al., 2009), we use ARTS to generate single scattering albedo, asymmetry parameter, absorption coefficient, and scattering phase functions for PSDs centered at a wide range of effective radii to create optical property lookup tables for each radiation code. The ARTS ice optical properties follow Yang et al. (2013), with updates according to Bi and Yang (2017) (Eriksson and Barlakas, 2024).

The spectral discretization of these properties matches the one requested by ecRad, with about 200 spectral points across both longwave and shortwave wavenumbers. Because cloud optical properties do not vary strongly with wavenumber, this spectral discretization is sufficient, and increasing it does not significantly change IRF (not shown). In harmonized radiation codes, then, differences in forcing estimates can arise only from differences in the spectral or angular discretization of the code, the gas optics scheme, or other implementation details (e.g., how the code treats model layers and their interfaces). The

https://doi.org/10.5194/egusphere-2026-6723
Preprint. Discussion started: 12 November 2026
© Author(s) 2026. CC BY 4.0 License.

| Code | Version | Type | Gas Optics | Spectral Detail | Streams | Notes |
|---|---|---|---|---|---|---|
| ARTS | Python interface `pyarts` v2.6.18 | line-by-line | HITRAN database (Gordon et al., 2022) | 50,000 wavenumbers | 10 streams | the Python module `FluxSimulator` v0.9 (https://github.com/atmtools/pyarts-fluxes) is used to run ARTS |
| libRadtran | 2.0.6 | intermediate complexity | REPTRAN (Gasteiger et al., 2014) | 15 $cm^{-1}$ bands | 16 streams | REPTRAN was developed using ARTS calculations as a reference, so libRadtran and ARTS are not fully independent. We use Python module `pyLRT` v0.2.2 (github.com/EdGrrr/pyLRT) to interface with libRadtran. |
| ecRad | 1.7.1 | correlated-$k$ | Default ecCKD: v1.4 (shortwave), v1.0 (longwave) | 32 $g$-points | 2 streams | — |
| RRTMGP | Python RTE-RRTMGP v0.2.5 | correlated-$k$ | Default correlated-$k$ | 256 LW / 224 SW $g$-points | 2 streams | Includes a patch to treat longwave scattering. |

**Table 1.** Details of the radiative transfer codes used in the intercomparison.

https://doi.org/10.5194/egusphere-2026-6723
Preprint. Discussion started: 12 November 2026
© Author(s) 2026. CC BY 4.0 License.

dominant effect is spectral discretization, as two-stream codes are optimized to reproduce multi-angular calculations with great accuracy under certain conditions (Ho and Pincus, 2024).

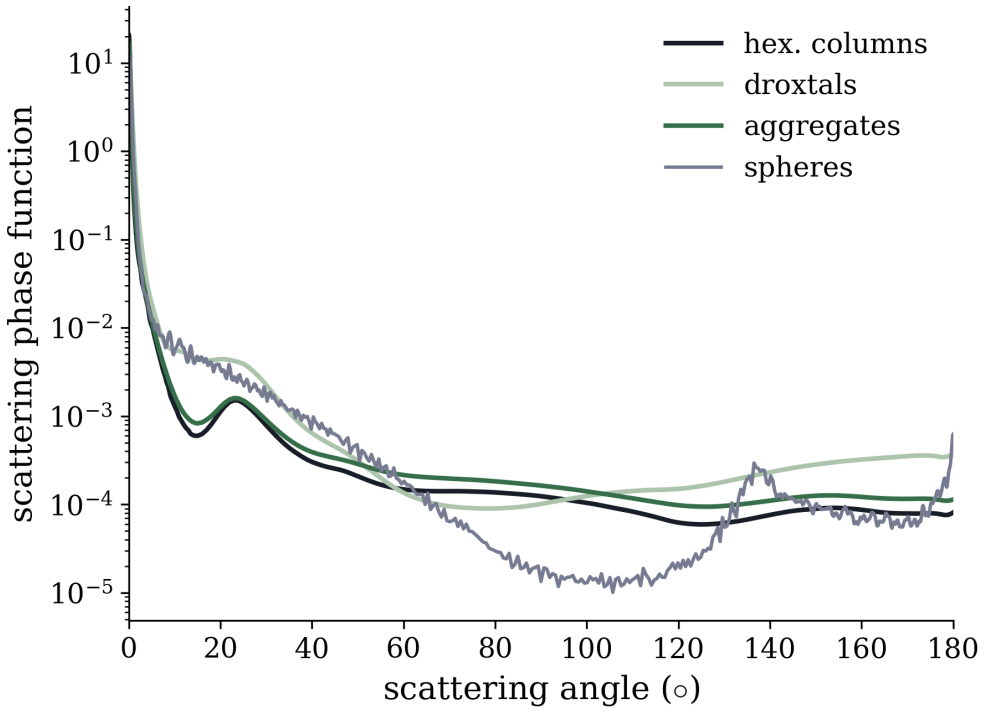



**Figure 1.** The scattering phase function at a wavelength of 0.55 $\mu$m for moderately-rough hexagonal columns (black), moderately-rough droxtals (light green), 8-column, moderately-rough aggregates (dark green), and Mie spheres (grey). The particle size distribution is chosen so that the effective radius is 15 $\mu$m.

To test the sensitivity of the uncertainty in IRF to the scattering phase function, we perform harmonization across four different particle shapes chosen to span common habits observed and modeled in thin ice clouds (Heymsfield et al., 2017; Ebert and Curry, 1992): hollow, moderately-rough hexagonal columns; moderately-rough droxtals; 8-column moderately-rough aggregates; and Mie spheres. The phase functions at $r_{\text{eff}} = 15$ $\mu$m and wavelength 0.55 $\mu$m for these four particle shapes are shown in Figure 1. Among the four habits, aggregates have the largest shortwave effect, as they scatter to space more strongly than the other shapes, while spheres side-scatter least and so exert a smaller shortwave forcing.

## 3 Idealized Contrails

Our idealized contrail radiative forcing benchmark follows Myhre et al. (2009). We begin with an International Standard Atmosphere with a surface temperature of 288 K (generated by the function `standard_atmosphere` from the Python package `typhon`, version 0.9.0). Greenhouse gas concentrations are fixed at present-day levels. In the longwave, the surface

https://doi.org/10.5194/egusphere-2026-6723
Preprint. Discussion started: 12 November 2026
© Author(s) 2026. CC BY 4.0 License.

is non-reflecting with an albedo of 0.01, and the shortwave surface albedo is fixed at 0.2. The contrail fills the full model level between 10 and 11 km of altitude (cloud fraction $f = 1$), where the temperature is about 217 K. The contrail optical thickness is $\tau = 0.3$, as in Myhre et al. (2009). The effective radius of the ice particles is 15 $\mu$m, a typical value for persistent contrails (Schumann et al., 2017; Li et al., 2023), and the ice optical properties are described in Section 2.1.1. In the radiative benchmark experiment, we show the IRF at solar zenith angles of 30°, 60°, and 75° for a default hexagonal column ice particle habit.

### 3.1 The Contrail Radiative Benchmark

In Figure 2, we present the results of the radiative benchmark experiment following Myhre et al. (2009). For each code, Figure 2 shows the IRF resulting from harmonization as well as for different code settings to explore the contribution of different configurations to overall diversity. One setting is changed at a time: either the default ice optics parameterization is used ("unharmonized"), or the harmonized ice optics are used but other code options are changed. The changes that produce a significant departure from the harmonized IRF are shown. In all, diversity due to radiative transfer code is much smaller when codes are *harmonized* (the same settings and ice parameterization is used) than when settings are varied.

Unharmonized differences in IRF are larger in magnitude than those reported by Myhre et al. (2009), while harmonizing optical properties significantly reduces code diversity. At a 30° solar zenith angle (Fig. 2c), using two streams rather than ten in ARTS (yellow) significantly increases the estimated net forcing, while using just 240 frequencies rather than the full 50,000 ("sparse") decreases the forcing (though the estimate remains within those provided by other codes). This relationship does not hold at the higher solar zenith angles, with unharmonized versions of ARTS matching the reference calculation fairly well at 60° in the shortwave (leading to a larger net effect; Fig. 2d, e). At $\theta = 75°$, the discrepancy grows, with the 2-stream version of ARTS providing the largest positive, outlying net forcing estimate (Fig. 2f, g).

Unharmonized RRTMGP (green) provides the smallest IRF of all the codes, as the default RRTMGP ice optics parameterization assumes a strongly back-scattering phase function. Turning off longwave scattering ("no lw. scatt.") decreases the longwave forcing estimate by about 3 W/m$^2$ in all of the unharmonized codes when compared to the harmonized codes. Changing how ecRad (blue) processes cloud optical properties (band-averaging, which is less accurate than the default per-$g$-point calculation; Hogan (2022)) causes an over-estimation of IRF magnitude in the longwave (Fig. 2a) that translates to a small under-estimation in the net (Fig. 2c, e, g), an effect that is consistent across solar zenith angle.

Finally, the CoCiP radiative forcing parameterization (purple), which is fit to libRadtran reference calculations (Schumann et al., 2012) but not harmonized, falls well within the distribution of unharmonized codes across solar zenith angle, though it is biased towards a more negative shortwave IRF when the sun is closer to zenith.

### 3.2 Sensitivity of Diversity to Cloud Properties

Next, we test how the agreement between radiation codes depends on cloud properties: contrail optical depth $\tau$, effective radius $r_{\text{eff}}$, ice particle habit, and a wider range of solar zenith angles. All ice optical properties are harmonized, and the background atmosphere and position of the cloud remain as in the Myhre experiment.

https://doi.org/10.5194/egusphere-2026-6723
Preprint. Discussion started: 12 November 2026
© Author(s) 2026. CC BY 4.0 License.

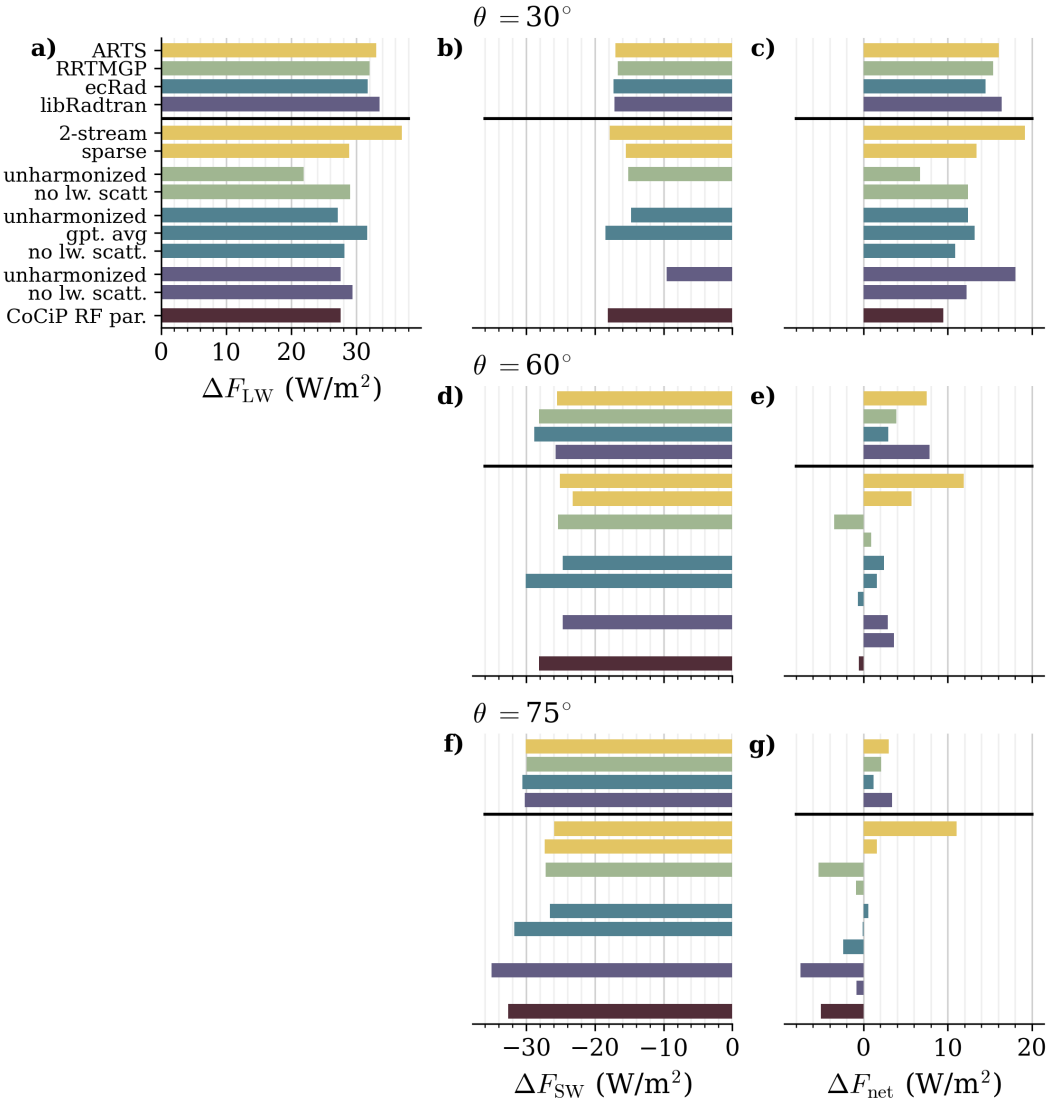



**Figure 2. a)** Instantaneous longwave, **b, d, f)** shortwave, and **c, e, g)** net radiative forcing (W/m$^2$) by a contrail with optical depth $\tau$ = 0.3 made up of hexagonal columns of effective radius $r_{\mathrm{eff}}$ = 15$\mu$m. Calculations are performed at solar zenith angles **b, c)** 30°, **d, e)** 60°, and **f, g)** 75°. Four radiation codes are used: ARTS (yellow), RRTMGP (green), ecRad (blue), libRadtran (purple), and the CoCiP radiative forcing parameterization is also shown (brown). Above the divider, they are harmonized, while below the divider different code settings (described in the text) are used.

The top row of Figure 3 shows the mean IRF across the four harmonized radiation codes, while the bottom row shows the diversity between the codes (Eqn. 1). The effective radius is 15 $\mu$m and optical depth ranges from very optically thin ($\tau = 0.05$) to very optically thick ($\tau = 1.5$), spanning observed values (Schumann et al., 2017).

https://doi.org/10.5194/egusphere-2026-6723
Preprint. Discussion started: 12 November 2026
© Author(s) 2026. CC BY 4.0 License.

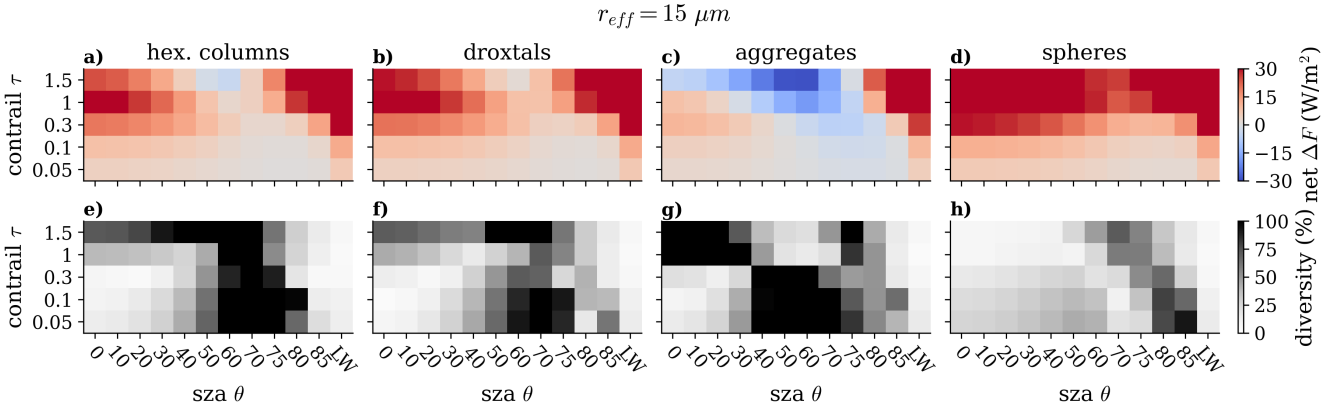



**Figure 3. a-d)** The mean instantaneous net contrail radiative forcing (W/m$^2$) and **e-h)** diversity (Eqn. 1) between four radiation codes across contrail optical thickness and solar zenith angle. **a, e)** assume the contrail ice particles are hexagonal columns, **b, f)** assume droxtals, **c, g)** assume aggregates, and **d, h)** spheres, all with $r_{\text{eff}}$ = 15 $\mu$m.

Figure 3 illustrates that both the sign of the forcing and the code diversity are driven by scattering properties. Longwave-only IRF (final column, Fig. 3a-d) is largely determined by cloud optical thickness, with the forcing magnitude varying little (within 2 W/m$^2$) across particle habit. The exception is $\Delta F_{LW}$ of contrails made up of aggregate particles (Fig. 3c), which is up to 12 W/m$^2$ smaller at $\tau = 1.5$ than other habits. This difference arises from our definition of effective radius which, when fixed at 15 $\mu$m, requires a smaller IWC to produce the same $\tau$ as the other particles. Nonetheless, even when accounting for this longwave difference, the sign of the forcing is driven by shortwave scattering. Spheres side-scatter the least and so have the most positive effect across a range of solar zenith angle (Fig. 3d, h; Fig. 1). Conversely, aggregates exhibit the most side scattering, closely followed by hexagonal columns (Fig. 1), explaining the negative forcing at higher solar zenith angles (Fig. 3c-d, g-f).

Diversity is largest where $\Delta F_{net}$ is near-zero, as the codes disagree where in the $(\tau, \theta)$ parameter space shortwave forcing outweighs longwave forcing. This is distinct from the amplification of $D$ via division by small mean[$\Delta F$]: note that in addition to the imposed lower bound on the denominator of $D$ (Eqn. 1), diversity is small where forcing is small because the cloud is optically thin (Fig. 3e-h).

Figure 4 shows the same metrics for a fixed effective radius of 30 $\mu$m. For a larger particle size, fewer particles are necessary to achieve the same optical depth and so scattering becomes less important to the net forcing; this is reflected in the more positive mean forcing across all $\tau$ and $\theta$ (Fig. 4a-d). Similarly, $D$ is smaller as the balance between positive and negative effects is more decisively dominated by the longwave (Fig. 4e-h). The exception are contrails made up of 30 $\mu$m aggregate particles, which exert a more positive forcing than the corresponding 15 $\mu$m contrails, and codes disagree on the optical thickness where the forcing switches sign from negative to positive.

https://doi.org/10.5194/egusphere-2026-6723
Preprint. Discussion started: 12 November 2026
© Author(s) 2026. CC BY 4.0 License.

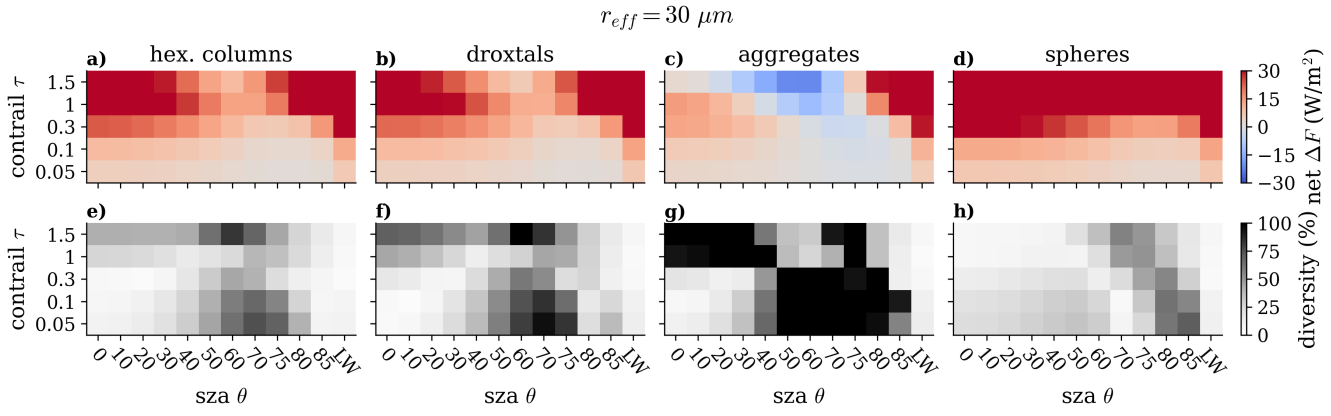



**Figure 4.** Same as Fig. 3, but with effective radius $r_{\text{eff}}$ = 30 $\mu$m.

## 4 Contrail Outbreak

We have shown that disagreement between radiation codes depends on the properties of the scene: the effective radius of the PSD, the optical thickness of the cloud, the ice habit, and the position of the sun. This raises the question: is the diversity systematic or random? In other words, will codes agree more or less strongly over a realistic set of contrail properties and solar zenith angles?

To answer these questions, we generate a more realistic set of contrail properties with CoCiP (using Python package `pycontrails` v0.63.1; Schumann, 2012). Because our aim is not to quantify the contrail radiative forcing but rather to generate a set of contrails with realistic properties over changing solar zenith angles and meteorological conditions, we use CoCiP's sample flight paths over the continental US to drive the creation of the clouds (Fig. 5a). The sample flights (available at https://apidocs.contrails.org/_static/fleet_sample.csv), which originally span about 4 hours from 8PM-midnight on 10 February 2023, are shifted to the summer 2019 solstice date and repeated to cover a 24-hour period. A single particle habit (hollow hexagonal columns) is enforced for more direct comparison with our harmonized radiation codes. We use radiation and meteorological variables from the ERA5 reanalysis dataset (Hersbach et al., 2023) on the summer solstice (21 June 2019) in 2019 in order to sample the largest distribution of solar zenith angles, and assume otherwise clear skies over the study area. The ice supersaturated regions (ISSRs) necessary to the formation of contrails, diagnosed by CoCiP from the meteorological reanalysis data, are shown in Fig. 5b.

CoCiP provides contrail properties at flight waypoints. In order to re-calculate the radiative forcing with radiation codes offline, we re-grid the output onto the 1-degree ERA5 grid and an hourly time grid. The ice water content in a gridbox is given by the contrail-volume-weighted-mean of the individual contrails' ice water content, and the effective radius is similarly weighted by both the contrails' volume and the IWC. Finally, because the data underlying the harmonized hexagonal column ice optics is limited to effective radii between 9 and 90 microns, we discard any contrails outside of this range ahead of averaging. This is a common limitation to ice optics parameterizations used in Earth systems models (Bock and Burkhardt, 2016).

https://doi.org/10.5194/egusphere-2026-6723
Preprint. Discussion started: 12 November 2026
© Author(s) 2026. CC BY 4.0 License.

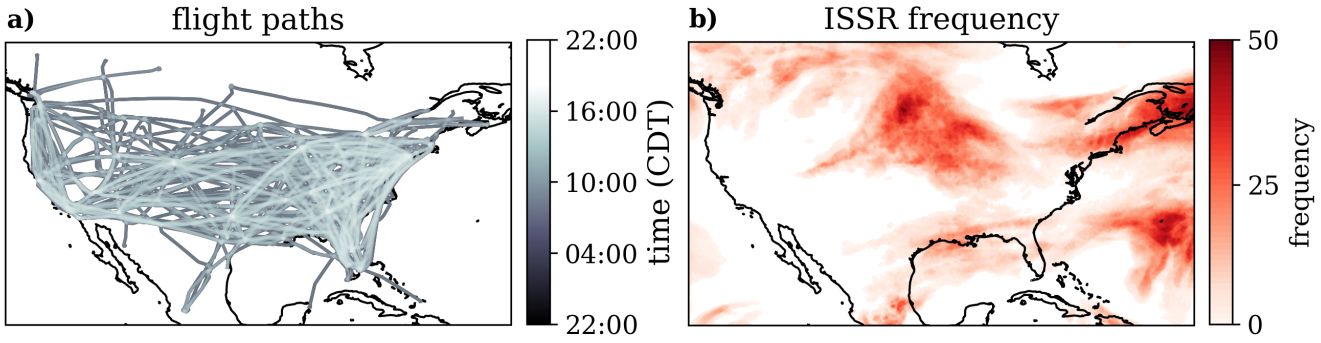



**Figure 5. a)** The flight paths colored by take-off time and **b)** the frequency of ice supersaturated regions over the 2019 summer solstice.

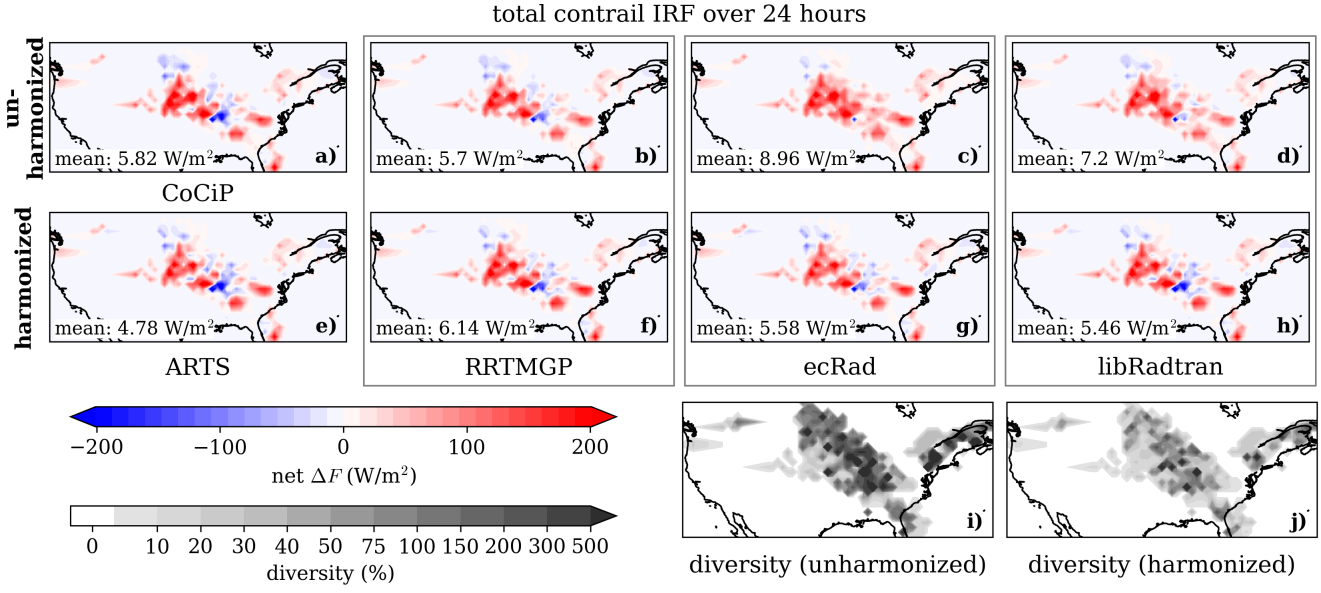



**Figure 6.** Total net instantaneous contrail radiative forcing (W/m$^2$) over a 24-hour summer solstice for a simulated contrail outbreak. Contrail properties are derived from CoCiP and then used by codes with original ice optical property parameterizations (**a)** CoCiP; **b)** RRTMGP; **c)** ecRad; and **d)** libRadtran) and harmonized properties (**e)** ARTS; **f)** RRTMGP; **g)** ecRad; and **h)** libRadtran). The diversity among unharmonized (**i**) and harmonized (**j**) codes is quantified.

The total net IRF over the 24-hour CoCiP run is shown in Figure 6. Both unharmonized (Fig. 6a-d) and harmonized (Fig. 6e-h) versions of the radiation codes largely agree on the sign and magnitude of the spatial distribution of the contrail IRF, though unharmonized ecRad (Fig. 6c) and libRadtran (Fig. 6d) estimate a less negative forcing. Conversely, the CoCiP radiative forcing parameterization displays good agreement with harmonized codes despite its fit to a different ice optics parameterization

https://doi.org/10.5194/egusphere-2026-6723
Preprint. Discussion started: 12 November 2026
© Author(s) 2026. CC BY 4.0 License.

(Fig. 6a). Quantitatively, harmonization decreases diversity (Fig. 6i-j). As in Section 3.2, $D$ is largest when codes disagree on the sign of the forcing, and consequently diversity is often largest in regions where the net magnitude of $\Delta F$ is small.

Next we analyze how the diversity between IRF estimates evolves with cloud properties and solar zenith angle across time in Figure 7. The domain-averaged effective radius (Fig. 7a, red) and contrail optical depth (Fig. 7a, grey) are roughly anti-correlated. The domain-averaged solar zenith angle is shown in Fig. 7c along with the time (Central Daylight Time zone).

The domain-averaged contrail IRF calculated by each code is shown in Fig. 7b. The CoCiP radiative forcing parameterization estimates a larger IRF at night compared to the other codes, and unharmonized ecRad and libRadtran estimate more positive forcing during the day compared to the other codes. This latter pattern can be interpreted with Fig. 2, which shows that unharmonized ecRad and libRadtran tend to calculate a larger-magnitude shortwave forcing compared to their harmonized versions at low solar zenith angles. The CoCiP parameterization calculates a smaller-magnitude longwave forcing compared to the harmonized codes for the set of parameters used in Fig. 2.

The total, domain- and time-averaged $\Delta F$ is shown within harmonized (black) and unharmonized (grey) codes, along with clouds indicating the maximum spread among codes. The mean forcing differs by about 2 W/m$^2$, at about 17 W/m$^2$ within the harmonized codes and 19 W/m$^2$ within the unharmonized codes. The harmonized codes agree within 11.1%, with a maximum spread of 1.88 W/m$^2$, while the unharmonized codes exhibit a larger diversity at 21.8%, or a maximum difference of 4.1 W/m$^2$. Both of these values are small compared to the diversity in harmonized codes in the idealized benchmarks (Fig. 3e), where the mean diversity is 62.5% across all combinations of parameters. Only 9 combinations of parameters yield diversity smaller than 11.1% in unharmonized codes (Fig. 3e, small optical thickness and either high solar zenith angle or longwave-only); about two-thirds of cases in the harmonized test (Fig. 3) display higher uncertainty than the unharmonized time- and domain-averaged diversity here. Therefore, we can conclude that the worst-case disagreement between codes in a realistic use case will be smaller than in individual benchmarks (about 10-20%), as disagreements compensate when averaging over space and time. We note, however, that this measure is sensitive to the time window over which the average is calculated, as the diversity will depend on the distribution of solar zenith angle over the averaging period. Averaging over the 24 hours of the summer solstice provides the widest range of solar zenith angle and longest daylight, and so a measure of the worst-case uncertainty due to scattering properties.

## 5 Summary and Conclusions

In this work, we evaluate the sensitivity of contrail cirrus radiative forcing to the choice of the code used to calculated the contrail and contrail-free radiative fluxes. We compare four widely-used radiative transfer codes, including a line-by-line code (ARTS), an intermediate-complexity code (libRadtran), two parameterizations used in Earth systems models (ecRad and RRTMGP), and the contrail radiative forcing parameterization used by the popular contrail prediction model CoCiP. We test the radiative transfer code diversity across a range of cloud properties in single-atmosphere cases and in a 24-hour run of CoCiP applied to realistic flight trajectories and real atmospheric conditions over the United States.

https://doi.org/10.5194/egusphere-2026-6723
Preprint. Discussion started: 12 November 2026
© Author(s) 2026. CC BY 4.0 License.

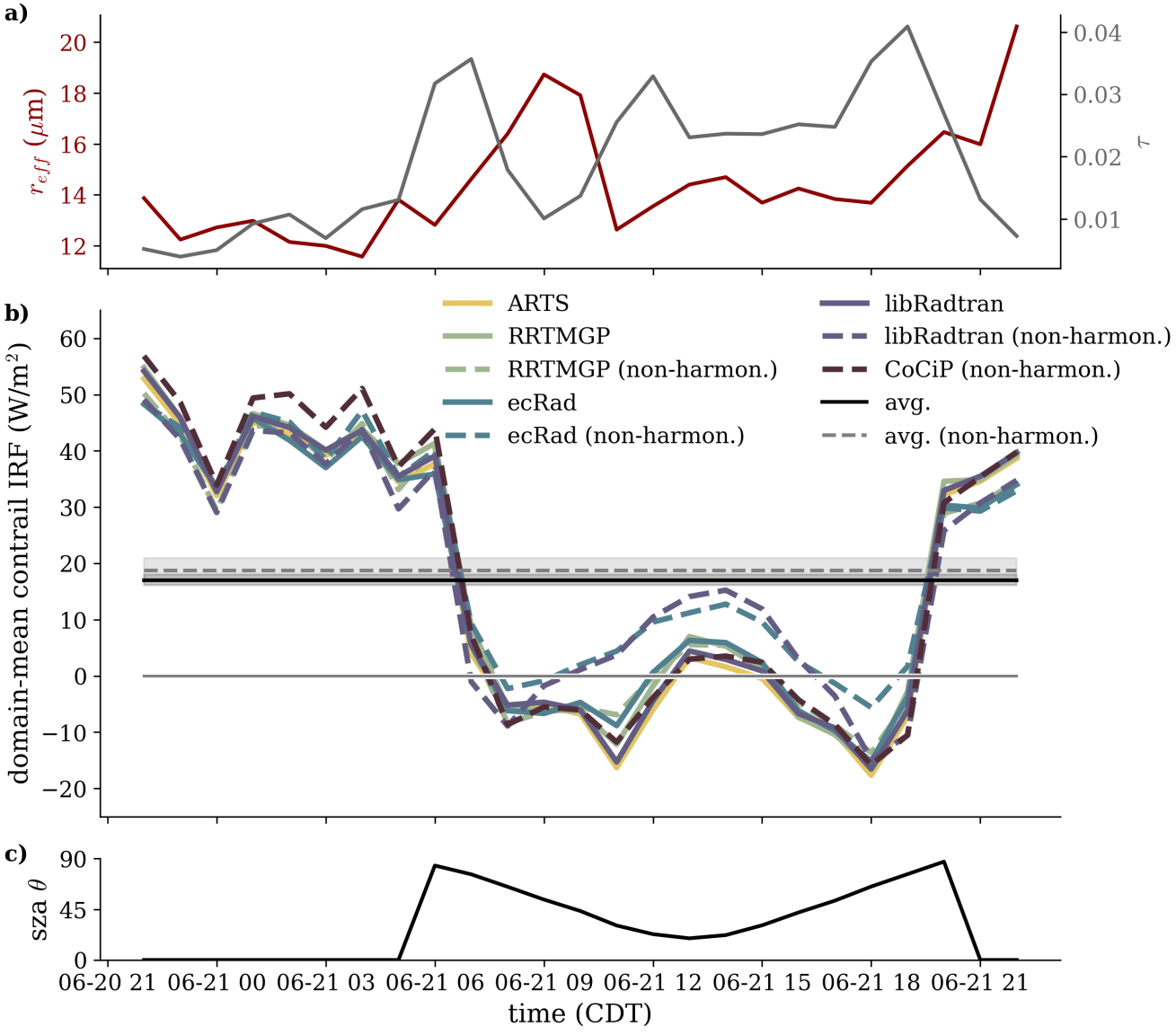



**Figure 7. a)** The domain-mean contrail properties over a contrail outbreak simulated by CoCiP with synthetic flights shifted to the summer solstice in 2019: effective radius (red) and gridbox-mean optical depth (grey). **b)** Domain-mean instantaneous contrail radiative forcing, using both harmonized (solid lines) and unharmonized (dashed lines) radiation codes. The temporal and spatial average among harmonized (black) and unharmonized (grey) codes is additionally shown, with shading spanning the maximum and minimum values predicted by the codes. **c)** The solar zenith angle at each Central Daylight Time.

We find that both the magnitude and sign of the contrail radiative forcing depend most strongly on ice optical properties. After "harmonizing", or imposing an identical ice optical parameterization across codes, diversity between codes is driven by

https://doi.org/10.5194/egusphere-2026-6723
Preprint. Discussion started: 12 November 2026
© Author(s) 2026. CC BY 4.0 License.

spectral discretization, with additional differences stemming from different angular resolution or other code implementation details. In the Myhre et al. (2009) benchmark, diversity in $\Delta F_{LW}$ is about 30% and the maximum shortwave diversity across the three solar zenith angles is 27%. In contrast, the longwave diversity is 5.6% in our harmonized codes and 22% in the unharmonized codes. In the shortwave, the maximum diversity among harmonized codes is 12%, while it reaches 55% in unharmonized codes. In the net, the largest diversity appears when the absolute magnitude of the forcing is small and the codes disagree on its sign. Because of the small net forcing values, this reaches 4000% in the Myhre et al. (2009) benchmark, 90% in our harmonized codes, and 2000% in our unharmonized codes. For this reason, the 35% uncertainty value reported in Myhre et al. (2009) and Lee et al. (2021) is the maximum diversity of longwave and shortwave IRF, rather than net IRF.

The type-A uncertainty (uncertainty due to contrail radiative response) in global contrail cirrus radiative forcing reported in Lee et al. (2021) is calculated as the root sum of the square of four sub-categories of uncertainty, among them the uncertainty due to the model's radiative transfer scheme (A1). If uncertainty A1 is updated with our re-assessment of 12% in modern, harmonized radiation codes in the radiative benchmark calculation (analogous to Myhre et al., 2009), type-A uncertainty decreases from 55% to about 45%. The overall uncertainty in contrail radiative forcing decreases from 70% to about 60%. (We follow Lee et al. (2021) in rounding our estimates up.)

Errors compensate when forcing is integrated over space or time, such that in a realistic use case, we attribute a diversity of about 11% stemming from the choice of radiation code, a similar value to the maximum benchmark value of 12% described above. If we consider the ice optical parameterization as a part of the radiation code, the diversity between codes rises to about 22%, with a maximum spread of about 4 W/m$^2$.

Together, these results separate uncertainty stemming from ice optical properties from uncertainty due to the radiative transfer code itself. Additionally, we show that the largest differences due to radiative transfer code are associated with the smallest-magnitude $\Delta F$, indicating IRF estimates are less sensitive to the choice of radiative transfer code where impacts are larger. In the context of contrail mitigation, this implies that identification of contrails to target for measures such as avoidance is insensitive to the choice of radiation code.

Here, the radiative forcing is calculated only in otherwise clear skies. Including natural cloud layers may increase disagreement between codes, as upwelling radiation would be mediated by the scattering properties of surrounding clouds. In addition to vertical overlap, contrails may form in the same model layer as natural cirrus, or embed in existing cirrus (Petzold et al., 2025; Seelig et al., 2025). Both of these phenomena may increase diversity due to differences in the mixing of optical properties of the two different cloud types, which is the topic of future work. Finally, in this work we focus on 1-D radiative transfer, but 3-D effects (horizontal photon transfer between individual atmospheric columns) can significantly change the contrail radiative forcing estimate, including changing its sign in some cases (Gounou and Hogan, 2007; Carles et al., 2025). This implies that 3-D effects would similarly increase uncertainty due to the choice of radiative transfer solver.

*Code and data availability.* Data, scripts, and code used for creating figures are available at 10.5281/zenodo.23601819 (Czarnecki et al., 2026).

https://doi.org/10.5194/egusphere-2026-6723
Preprint. Discussion started: 12 November 2026
© Author(s) 2026. CC BY 4.0 License.

*Author contributions.* P.C. conducted the analysis, led the investigation, created the visualizations and wrote the manuscript. All authors contributed to the conceptualization of the study. N.B. and O.B. supervised the research, reviewed and edited the manuscript, and acquired the funding enabling the work.

*Competing interests.* The authors declare no competing interests.

*Acknowledgements.* We thank Kevin Wolf for helpful discussion around the presentation of results and use of libRadtran code. This research has been supported by the French Ministere de la Transition Ecologique et Solidaire under the Climaviation project (grant DGAC N2021-39), with support from France's Plan National de Relance et de Resilience (PNRR) and the European Union's NextGenerationEU. This study benefited from the IPSL mesocenter ESPRI facility which is supported by CNRS, Sorbonne Université, Labex L-IPSL, CNES and École Polytechnique.

https://doi.org/10.5194/egusphere-2026-6723
Preprint. Discussion started: 12 November 2026
© Author(s) 2026. CC BY 4.0 License.

## References

Baran, A. J.: From the single-scattering properties of ice crystals to climate prediction: A way forward, Atmospheric Research, 112, 45–69, https://doi.org/10.1016/j.atmosres.2012.04.010, 2012.

Bi, L. and Yang, P.: Improved ice particle optical property simulations in the ultraviolet to far-infrared regime, Journal of Quantitative Spectroscopy and Radiative Transfer, 189, 228–237, https://doi.org/10.1016/j.jqsrt.2016.12.007, 2017.

Bock, L. and Burkhardt, U.: Reassessing properties and radiative forcing of contrail cirrus using a climate model, Journal of Geophysical Research: Atmospheres, 121, 9717–9736, https://doi.org/10.1002/2016JD025112, 2016.

Buehler, S. A., Larsson, R., Lemke, O., Pfreundschuh, S., Brath, M., Adams, I., Fox, S., Roemer, F. E., Czarnecki, P., and Eriksson, P.: The atmospheric radiative transfer simulator ARTS, version 2.6—Deep Python integration, Journal of Quantitative Spectroscopy and Radiative Transfer, p. 109443, https://doi.org/10.1016/j.jqsrt.2025.109443, 2025.

Carles, J., Bellouin, N., Villefranque, N., and Dufresne, J.-L.: The subtleties of three-dimensional radiative effects in contrails and cirrus clouds, Atmospheric Chemistry and Physics, 25, 13 953–13 973, https://doi.org/10.5194/acp-25-13953-2025, 2025.

Chen, T., Rossow, W. B., and Zhang, Y.: Radiative effects of cloud-type variations, Journal of climate, 13, 264–286, https://doi.org/10.1175/1520-0442(2000)013<0264:REOCTV>2.0.CO;2, 2000.

Czarnecki, P., Boucher, O., and Bellouin, N.: pczarnecki/code-diversity-paper-figures: zenodo, https://doi.org/10.5281/zenodo.23601819, 2026.

Ebert, E. E. and Curry, J. A.: A parameterization of ice cloud optical properties for climate models, Journal of Geophysical Research: Atmospheres, 97, 3831–3836, https://doi.org/10.1029/91JD02472, 1992.

Emde, C., Buras-Schnell, R., Kylling, A., Mayer, B., Gasteiger, J., Hamann, U., Kylling, J., Richter, B., Pause, C., Dowling, T., et al.: The libRadtran software package for radiative transfer calculations (version 2.0.1), Geoscientific Model Development, 9, 1647–1672, https://doi.org/10.5194/gmd-9-1647-2016, 2016.

Eriksson, P. and Barlakas, V.: Single scattering properties of ice hydrometeors between 0.2 and 99 um (Bi and Yang, 2017), https://doi.org/10.5281/zenodo.10807525, 2024.

Fu, Q. and Liou, K.: On the correlated $k$-distribution method for radiative transfer in nonhomogeneous atmospheres, Journal of the Atmospheric Sciences, 49, 2139–2156, https://doi.org/10.1175/1520-0469(1992)049<2139:OTCDMF>2.0.CO;2, 1992.

Gasparini, B., Meyer, A., Neubauer, D., Münch, S., and Lohmann, U.: Cirrus cloud properties as seen by the CALIPSO satellite and ECHAM-HAM global climate model, Journal of Climate, 31, 1983–2003, https://doi.org/10.1175/JCLI-D-16-0608.1, 2018.

Gasteiger, J., Emde, C., Mayer, B., Buras, R., Buehler, S., and Lemke, O.: Representative wavelengths absorption parameterization applied to satellite channels and spectral bands, Journal of Quantitative Spectroscopy and Radiative Transfer, 148, 99–115, https://doi.org/10.1016/j.jqsrt.2014.06.024, 2014.

Gordon, I., Rothman, L., Hargreaves, R., Hashemi, R., Karlovets, E., Skinner, F., Conway, E., Hill, C., Kochanov, R., Tan, Y., et al.: The HITRAN2020 molecular spectroscopic database, Journal of Quantitative Spectroscopy and Radiative Transfer, 277, 107 949, https://dx.doi.org/10.1016/j.jqsrt.2021.107949, 2022.

Gounou, A. and Hogan, R. J.: A sensitivity study of the effect of horizontal photon transport on the radiative forcing of contrails, Journal of the atmospheric sciences, 64, 1706–1716, https://doi.org/10.1175/JAS3915.1, 2007.

https://doi.org/10.5194/egusphere-2026-6723
Preprint. Discussion started: 12 November 2026
© Author(s) 2026. CC BY 4.0 License.



Hersbach, H., Bell, B., Berrisford, P., Biavati, G., Horányi, A., Muñoz Sabater, J., Nicolas, J., Peubey, C., Radu, R., Rozum, I., et al.: ERA5 monthly averaged data on single levels from 1940 to present [Dataset]. Copernicus Climate Change Service (C3S) Climate Data Store (CDS), https://doi.org/10.1002/qj.4803, 2023.

Heymsfield, A. J., Krämer, M., Luebke, A., Brown, P., Cziczo, D. J., Franklin, C., Lawson, P., Lohmann, U., McFarquhar, G., Ulanowski, Z., et al.: Cirrus clouds, Meteorological Monographs, 58, 2–1, https://doi.org/10.1175/AMSMONOGRAPHS-D-16-0010.1, 2017.

Ho, D. J. and Pincus, R.: Two-streams revisited: General equations, exact coefficients, and optimized closures, Journal of Advances in Modeling Earth Systems, 16, e2024MS004 504, https://doi.org/10.1029/2024MS004504, 2024.

Hogan, R. J.: ECRAD radiation scheme: User Guide, Document version, 1, https://confluence.ecmwf.int/spaces/ECRAD/overview?preview=/70945505/114525750/ecrad_documentation.pdf, 2022.

Hogan, R. J. and Bozzo, A.: ECRAD: A new radiation scheme for the IFS, vol. 787, European Centre for Medium-Range Weather Forecasts Reading, UK, https://doi.org/10.21957/whntqkfdz, 2016.

Hogan, R. J. and Bozzo, A.: A flexible and efficient radiation scheme for the ECMWF model, Journal of Advances in Modeling Earth Systems, 10, 1990–2008, https://doi.org/10.1029/2018MS001364, 2018.

Hogan, R. J. and Matricardi, M.: Evaluating and improving the treatment of gases in radiation schemes: the Correlated $K$-Distribution Model Intercomparison Project (CKDMIP), GMD, 13, 6501–6521, https://doi.org/10.5194/gmd-13-6501-2020, 2020.

Lacis, A. A. and Oinas, V.: A description of the correlated $k$-distribution method for modeling nongray gaseous absorption, thermal emission, and multiple scattering in vertically inhomogeneous atmospheres, Journal of Geophysical Research: Atmospheres, 96, 9027–9063, https://doi.org/10.1029/90JD01945, 1991.

Lee, D. S., Fahey, D. W., Skowron, A., Allen, M. R., Burkhardt, U., Chen, Q., Doherty, S. J., Freeman, S., Forster, P. M., Fuglestvedt, J., et al.: The contribution of global aviation to anthropogenic climate forcing for 2000 to 2018, Atmospheric environment, 244, 117 834, https://doi.org/10.1016/j.atmosenv.2020.117834, 2021.

Li, Y., Mahnke, C., Rohs, S., Bundke, U., Spelten, N., Dekoutsidis, G., Groß, S., Voigt, C., Schumann, U., Petzold, A., et al.: Upper-tropospheric slightly ice-subsaturated regions: frequency of occurrence and statistical evidence for the appearance of contrail cirrus, Atmospheric Chemistry and Physics, 23, 2251–2271, https://doi.org/10.5194/acp-23-2251-2023, 2023.

Liou, K.-N.: Influence of cirrus clouds on weather and climate processes: A global perspective, Monthly Weather Review, 114, 1167–1199, https://doi.org/10.1175/1520-0493(1986)114<1167:IOCCOW>2.0.CO;2, 1986.

Mauritsen, T., Tsushima, Y., Meyssignac, B., Loeb, N. G., Hakuba, M., Pilewskie, P., Cole, J., Suzuki, K., Ackerman, T. P., Allan, R. P., et al.: Earth's energy imbalance more than doubled in recent decades, Agu Advances, 6, e2024AV001 636, https://doi.org/10.1029/2024AV001636, 2025.

Mayer, B. and Kylling, A.: The libRadtran software package for radiative transfer calculations-description and examples of use, Atmospheric Chemistry and Physics, 5, 1855–1877, https://doi.org/10.5194/acp-5-1855-2005, 2005.

Myhre, G., Kvalevåg, M., Raedel, G., Cook, J., Shine, K. P., Clark, H., Karcher, F., Markowicz, K., Kardas, A., Wolkenberg, P., et al.: Intercomparison of radiative forcing calculations of stratospheric water vapour and contrails, Meteorologische Zeitschrift (Berlin), 18, https://doi.org/10.1127/0941-2948/2009/0411, 2009.

Petty, G. W. and Huang, W.: The modified gamma size distribution applied to inhomogeneous and nonspherical particles: Key relationships and conversions, Journal of the Atmospheric Sciences, 68, 1460–1473, https://doi.org/10.1175/2011JAS3645.1, 2011.

Petzold, A., Khan, N. F., Li, Y., Spichtinger, P., Rohs, S., Crewell, S., Wahner, A., and Krämer, M.: Most long-lived contrails form within cirrus clouds with uncertain climate impact, Nature Communications, 16, 9695, https://doi.org/10.1038/s41467-025-65532-2, 2025.

https://doi.org/10.5194/egusphere-2026-6723
Preprint. Discussion started: 12 November 2026
© Author(s) 2026. CC BY 4.0 License.



Pincus, R., Mlawer, E. J., and Delamere, J. S.: Balancing accuracy, efficiency, and flexibility in radiation calculations for dynamical models, Journal of Advances in Modeling Earth Systems, 11, 3074–3089, https://doi.org/10.1029/2019MS001621, 2019.

Pincus, R., Buehler, S. A., Brath, M., Crevoisier, C., Jamil, O., Franklin Evans, K., Manners, J., Menzel, R. L., Mlawer, E. J., Paynter, D., et al.: Benchmark calculations of radiative forcing by greenhouse gases, Journal of Geophysical Research: Atmospheres, 125, e2020JD033 483, https://doi.org/10.1029/2020JD033483, 2020.

Schumann, U.: A contrail cirrus prediction model, Geoscientific Model Development, 5, 543–580, https://doi.org/10.5194/gmd-5-543-2012, 2012.

Schumann, U., Mayer, B., Graf, K., and Mannstein, H.: A parametric radiative forcing model for contrail cirrus, Journal of Applied Meteorology and Climatology, 51, 1391–1406, https://doi.org/10.1175/JAMC-D-11-0242.1, 2012.

Schumann, U., Baumann, R., Baumgardner, D., Bedka, S. T., Duda, D. P., Freudenthaler, V., Gayet, J.-F., Heymsfield, A. J., Minnis, P., Quante, M., et al.: Properties of individual contrails: a compilation of observations and some comparisons, Atmospheric Chemistry and Physics, 17, 403–438, https://doi.org/10.5194/acp-17-403-2017, 2017.

Seelig, T., Wolf, K., Bellouin, N., and Tesche, M.: Quantification of the radiative forcing of contrails embedded in cirrus clouds, Nature Communications, 16, 10 703, https://doi.org/10.1038/s41467-025-66231-8, 2025.

Smith, J. R., Grobler, C., Hodgson, P. J., Mukhopadhaya, J., Shapiro, M. L., Mirolo, M., Stettler, M. E., Eastham, S. D., and Barrett, S. R.: The climate opportunities and risks of contrail avoidance, Nature communications, 17, 2092, https://doi.org/10.1038/s41467-026-68784-8, 2026.

Teoh, R., Schumann, U., and Stettler, M. E.: Beyond contrail avoidance: Efficacy of flight altitude changes to minimise contrail climate forcing, Aerospace, 7, 121, https://doi.org/10.3390/aerospace7090121, 2020.

Wang, Z., Bugliaro, L., Jurkat-Witschas, T., Heller, R., Burkhardt, U., Ziereis, H., Dekoutsidis, G., Wirth, M., Groß, S., Kirschler, S., et al.: Observations of microphysical properties and radiative effects of a contrail cirrus outbreak over the North Atlantic, Atmospheric Chemistry and Physics, 23, 1941–1961, https://doi.org/10.5194/acp-23-1941-2023, 2023.

Wolf, K., Bellouin, N., and Boucher, O.: Sensitivity of cirrus and contrail radiative effect on cloud microphysical and environmental parameters, Atmospheric Chemistry and Physics, 23, 14 003–14 037, https://doi.org/10.5194/acp-23-14003-2023, 2023.

Yang, P., Bi, L., Baum, B. A., Liou, K.-N., Kattawar, G. W., Mishchenko, M. I., and Cole, B.: Spectrally Consistent Scattering, Absorption, and Polarization Properties of Atmospheric Ice Crystals at Wavelengths from 0.2 to 100 $\mu$m, Journal of the Atmospheric Sciences, 70, 330–347, https://doi.org/10.1175/JAS-D-12-039.1, 2013.

Zhang, Y., Macke, A., and Albers, F.: Effect of crystal size spectrum and crystal shape on stratiform cirrus radiative forcing, Atmospheric Research, 52, 59–75, https://doi.org/10.1016/S0169-8095(99)00026-5, 1999.